Discover Geoscience

RESEARCH Open Access

Predicting sea level variations for early warning using SARIMA model and deep learning techniques in the northwest Arabian Gulf

Abather Jabbar Bashar Alhallaf[1,3*], J Vilcáez[1], Pratyaydipta Rudra[2] and Ali A. Lafta[3]

*Correspondence:
Abather Jabbar Bashar Alhallaf
aalhall@okstate.edu
[1]Boone Pickens School of Geology, Oklahoma State University, Stillwater, Ok 74078, USA
[2]Department of Statistics, Oklahoma State University, Stillwater, Ok 74078, USA
[3]Marine Science Center, University of Basrah, Basrah, Iraq

Abstract

Predicting sea level variations (SLV) in coastal areas is essential for flood warnings, environmental protection, and infrastructure management. While sea level forecasting has been studied in various parts of the Arabian Gulf, limited research exists on water level prediction for Iraqi coastal waters. This study applies traditional statistical models, including the Autoregressive Integrated Moving Average (ARIMA) and Advanced Seasonal ARIMA (SARIMA), alongside advanced deep learning techniques, such as Convolutional Neural Networks (CNN), Long Short-Term Memory (LSTM) networks, and a hybrid CNN-LSTM model, to predict sea level variations in the northwest Arabian Gulf. The results demonstrate that ARIMA provides poor predictions, while SARIMA offers better forecasts with MSE = 0.0265, RMSE = 0.1626, and MAE = 0.1288. However, deep learning models, particularly CNN-LSTM, significantly outperform traditional models, with CNN achieving MSE = 0.0191, RMSE = 0.1384, and MAE = 0.1126, LSTM achieving MSE = 0.0172, RMSE = 0.1311, and MAE = 0.1055, and CNN-LSTM achieving MSE = 0.0165, RMSE = 0.1282, and MAE = 0.1015. This research highlights the potential of deep learning techniques for more reliable sea level predictions and improved flood risk management, emphasizing their advantage over conventional statistical methods.

Keywords Time series analysis, SLV, ARIMA, SARIMA, CNN, LSTM, MSE, RMSE

1 Introduction

Sea level rise presents a significant risk to coastal communities globally, underscoring the necessity for enhanced prediction models to alleviate the detrimental impacts of coastal flooding and to create effective adaptation strategies [1–3]. Floods and sea level rise are closely associated in terms of climate change, with rising sea levels enhancing the probability of flooding in coastal cities. Many regions, including the Arabian Gulf, could experience a potential doubling in flood frequency by 2050 because of rising sea levels, according to frequency analysis employing the Generalized Extreme Value (GEV) distribution [4]. Recent studies predict considerable regional sea level rise in the Arabian Gulf, estimating significant increases in total water levels by mid-century [5].

Coastal areas globally experience sea-level variations over a wide range of temporal scales, ranging from seconds to millennia. The Arabian Gulf is particularly vulnerable to these changes due to its distinctive physical characteristics. A semi-enclosed body of water extending 990 km in length and up to 370 km in width, with an average depth of roughly 36 m [6]. Moreover, the Arabian Gulf is as an essential channel for worldwide oil transportation, attracting significant attention from scholars in other scientific disciplines. The significance of this issue for both strategic and environmental reasons has led to extensive research, especially in oceanographic studies focused on understanding and reducing the effects of sea-level fluctuations, along with other marine and ecological challenges [7–9].

Despite its economic significance, the region remains vulnerable to extreme events. A recent catastrophic occurrence occurred on March 19, 2017. This event was a meteorological tsunami [10] that impacted the shorelines of Dayyer coastal city along the northern coast of the Gulf [11]. During this occurrence, the highest run-up reached 3 m, with the flooding extending approximately one kilometer inland, resulting in five fatalities. This unfortunate event highlights the critical necessity for enhanced comprehension and forecasting of sea-level fluctuations in the area.

Several studies have examined sea-level variability in the Arabian Gulf. In the study conducted by Sharaf El Din (1990), it is shown that sea levels along the western coast are typically lower in winter and higher in spring and summer [12]. Sultan et al. (1995) indicated that about 75% of sea level change on the Saudi coast was attributed to atmospheric pressure fluctuations [13]. Hosseinibalam (2007)showed that 62-90.2% of the seasonal fluctuations in sea level are caused by atmospheric pressure on the Iranian side [14]. At Juaymah on the west coast, Al-Subhi [15] demonstrated that 90% of annual variations of sea levels are due to astronomical tide [15]. In a research by Lafta (2019) on the northwest point of the Arabian Gulf, the characteristics of the tidal wave in Khor Al-Zubair and Khor Abdullah were examined, revealing that approximately 96% of annual variations are attributed to the astronomical tide [16]. Recent studies have utilized predictive modeling to improve the understanding of sea-level dynamics in the Arabian Gulf. Alenezi et al. [17] utilized Artificial Neural Networks (ANNs), particularly the Long Short-Term Memory (LSTM) model, to forecast sea levels in Mina Salman, successfully filling data gaps and achieving high accuracy [17]. Elneel et al. [18] employed ARIMA and Prophet models to predict regional sea levels, demonstrating that the Arabian Gulf exhibits greater fluctuations compared to global averages [18]. Although recent modeling efforts such as those by Alenezi et al. [17] and Elneel et al. [18] have employed advanced time series techniques for SLV forecasting in the Arabian Gulf, there remains a critical research gap: the lack of comparative studies evaluating both traditional statistical and deep learning models in the northwestern Gulf, particularly near the Iraqi coastline. Furthermore, SARIMA has been underutilized in this region, especially in combination with high-resolution time series data to assess its seasonal forecasting capability against more complex neural networks.

This study aims to fill this gap by developing and comparing the performance of SARIMA and deep learning models (LSTM, CNN, and CNN-LSTM) using in-situ sea-level data collected from the northwest Arabian Gulf. The SARIMA model is optimized to account for seasonality and autocorrelation, while deep learning models are employed to capture nonlinear and long-term dependencies. The findings will not only evaluate

the practical limitations of SARIMA in this context but also demonstrate the potential of hybrid deep learning models for improving early warning systems in climate-sensitive coastal regions.

The implications of this research are both scientific and practical: it improves our understanding of regional sea-level dynamics and provides critical input for disaster preparedness, coastal infrastructure planning, and flood mitigation efforts under climate change. Figure 1 shows the flowchart of the research.

2 Forecasting methods

2.1 Classical time-series forecasting methods (ARIMA) (SARIMA)

ARIMA is a powerful model for time series analysis and forecasting, and it has demonstrated successful application in various domains, such as forecasting tourism demand [19] and predicting vehicular traffic flow [20]. The Autoregressive Integrated Moving Average (ARIMA) model, often recognized as the Box-Jenkins time series model, is implemented through a systematic approach known as the Box–Jenkins method [21]. This method entails identifying, fitting, checking, and utilizing ARIMA models based on statistical tools such as the autocorrelation function (ACF), partial autocorrelation function (PACF), extended autocorrelation function (EACF), and Augmented Dickey-Fuller unit root test (ADF) to determine the stationarity of the variable under consideration and the lag lengths of the ARIMA model. The ARIMA model encompasses subclasses of other models, including Autoregressive (AR) [22], Moving Average (MA), and Autoregressive Moving Average (ARMA) models [22].

The Box-Jenkins method assumes that the process generating the time series can be estimated using either an Autoregressive Moving Average (ARMA) model or an Autoregressive Integrated Moving Average (ARIMA) model, depending on the stationarity of the data. However, when confronted with data exhibiting seasonal patterns, the Seasonal Autoregressive Integrated Moving Average (SARIMA) model is often more suitable, as it incorporates additional terms to address seasonality [23].

The accuracy of ARIMA predictions tends to be higher for short- to medium-term forecasts, typically up to one or two seasonal periods ahead. This is because the model is able to capture the seasonality and short-term fluctuations in the data quite well. However, as the forecasting horizon increases beyond a few seasonal periods, the accuracy of the predictions tends to degrade and become less reliable [24].

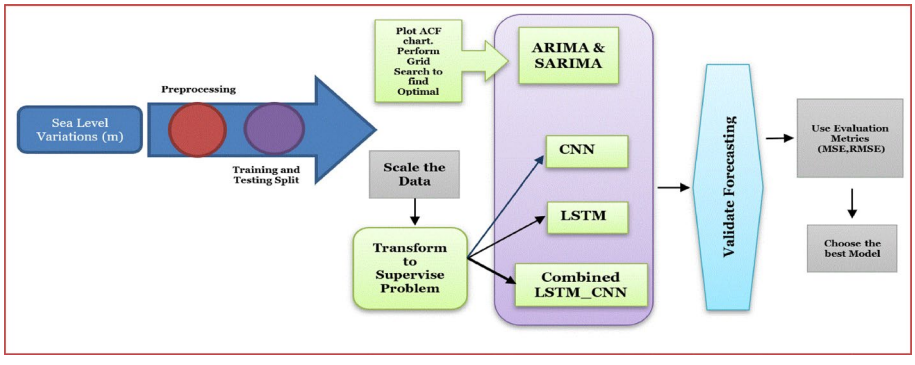

Fig. 1 The flow chart of the research

2.2 Deep learning methods

Artificial intelligence (AI) offers a diverse toolbox for tackling various challenges [25–27]. Machine learning (ML), a subset of AI, plays a key role in forecasting and decision-making by analyzing sample data (training data) without explicit programming [28, 29]. Deep learning (DL) takes ML a step further, empowering neural networks with memory capabilities. This allows them to learn from past inputs and identify complex patterns [30, 31].

Multilayer Perceptrons (MLPs) with added hidden layers are fundamental in deep neural networks allowing them to model more complex functions [32]. This triumphant method based on Artificial Neural Networks (ANNs) has seen applications in solar power forecasting [33], stock prices [34], and short-term traffic [35].

Convolutional Neural Networks (CNNs) are a recent addition to the deep learning toolbox for time-series forecasting. Similar to MLPs, CNNs consist of interconnected layers with learning capabilities [36]. Information processing occurs layer by layer, culminating in the network's forecast at the output layer. Despite similarities to MLPs [37], CNNs differ in how they handle input data. Images, for example, are typically represented as two-dimensional matrices [37]. While adding more neurons and layers to MLPs allows for complex models, this can lead to expensive computations and overfitting. Conversely, CNNs preserve the input structure, focusing on the relationships between neighboring pixels [38]. Koprinska et al. examined CNNs for short-term solar energy and electricity forecasts, proving their advantage over MLPs [39]. Similarly, Momeny et al. developed a robust CNN-based method [40], and Sorkhabi et al. employed CNNs to predict dynamic sea-level variability, revealing a strong positive spatial correlation between Sea Surface Temperature (SST) and Sea Surface Height (SSH) near the Gothenburg coast [41].

Recurrent Neural Networks (RNNs) are another powerful deep learning method gaining traction. Their looped architecture allows them to retain information from past events, making them well-suited for time-series predictions [42]. Long Short-Term Memory (LSTM) networks, a specific type of RNN, excel at learning long-term dependencies. Unlike standard RNNs where memorization is an additional skill, LSTMs are inherently designed to remember information for extended periods [43–45]. These networks consist of interconnected modules that process information in a unique way, ultimately proving valuable for sea water level prediction tasks, as demonstrated by [41, 46]. More recently, hybrid deep learning architectures combining CNNs and LSTMs have shown significant promise in improving sea-level forecasting accuracy. For example, Uluocak (2025) conducted a comparative study demonstrating that CNN-LSTM models outperformed standalone models in predicting global sea-level rise through 2050, using historical sea-level observations and climate model-based air temperature projections [47]. Likewise, a 2025 study on air pollution forecasting in Türkiye utilized hybrid CNN-LSTM and CNN-GRU architectures to predict daily NO_2 concentrations in Istanbul and Ankara, achieving superior performance compared to traditional models such as ARMA, ANN, and ANFIS-FCM [48]. These findings collectively underscore the versatility and effectiveness of hybrid deep learning models for both marine and atmospheric environmental forecasting applications.

3 Contributions to research

The main research findings from this paper are as follows:

- Utilized diverse forecasting methodologies, including statistical techniques like ARIMA, to predict water levels entirely based on historical sea level data. Furthermore, we employed statistical methodologies such as SARIMA, which incorporates a seasonal component. We employed deep learning methodologies, particularly LSTM networks and CNNs, for predicting water levels exclusively using historical sea level data.
- Enhanced water level prediction accuracy by integrating CNN and LSTM architectures into a modified deep learning model.
- Employed established measures, including MSE, RMSE, and MAE, to statistically assess and compare the efficacy of various forecasting techniques.
- Identified the most effective forecasting methods, emphasizing the benefits and limitations of statistical and deep learning approaches. This guidance assists decision-makers in determining the best model based on data features and prediction complexity.

4 Study area and data collection

This study focuses on the Khor Abdullah lagoon, which is situated at the westernmost point of the Arabian Gulf (Fig. 2) [49]. This area extends for 40Km in the NW-SE direction. In the southeast, at the Arabian Gulf opening, it is 17Km wide, but it narrows northward to around 6.5 Km at Khor Bobian. To the east, it is bounded by Al-Faw Peninsula, and to the west by the Bobian Island. The depth of the Khor Abdullah lagoon ranges between 7 and 14 m, and averages at 10 m [50].

The study area is dominated by three tidal regimes with different tidal periods, namely diurnal, semidiurnal, and mixed tides. The tidal range is around 1 m. The highest tidal ranges area associated with strong tidal currents that that can reach velocities exceeding 0.5 m/s [51].

The region has an arid desert environment with two distinct seasons: the summer, which is hot and long and lasts for roughly 230 days, and the winter, which is cold and rainy. There are two main wind patterns in the study area: northwest winds, which

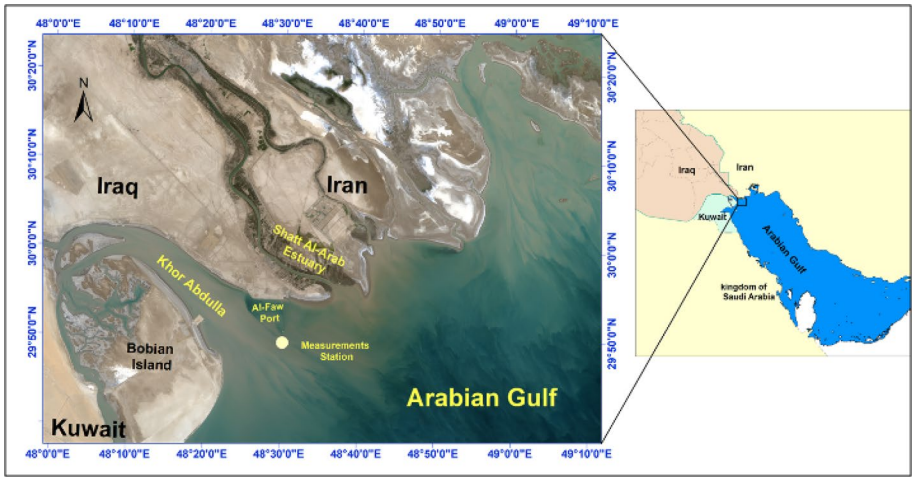

Fig. 2 The map of the study area with pointing on the measurement station [54]

periodically bring rainy clouds and generate dust storms in the summer and are locally known as "Al- Shammal", and southeast winds, which predominately blow during the fall and winter, which are typically warm and humid and occasionally bring clouds that rain [52].

Tidal measurements in Iraq's marine waters are extremely rare, and even when they had been measured, they are usually only available for brief periods of time. Fortunately, an offshore measurement platform was established at a distance of around 655 m from the western breakwater of Faw Grand Port by the General Company of Iraq Ports and DAE- WOO engineering and construction company. This station continuously records a number of oceanographic and meteorological variables. The General Acoustics company in Germany.

(https://www.generalacoustics.com) is in charge of managing this data. To the best of our knowledge, no other dataset has ever been located in the area, making this one special [53]. Over a 7-year period (2016–2022), the sea level variations (SLV). The continuous data records were taken at 10-minute intervals from 2016 to 2022.

4.1 Data pre-processing

The success of time series forecasting projects hinges on effective data pre-processing techniques [55]. In this study, we leverage time series aggregation, a well-established approach that demonstrably reduces computational resource requirements while potentially improving forecasting accuracy. Given the inherent high-frequency fluctuations observed in the all dataset collected at 10-minute intervals, a resampling strategy was employed to convert the data to daily frequency Fig. 2. This resampling utilized the method of averages, whereby the daily data value represents the arithmetic mean of the corresponding 10-minute measurements within that 24-hour period Fig. 3.

4.2 Assessment of forecast accuracy

The effectiveness of time-series forecasting models is gauged by various performance metrics, reflecting their predictive capabilities. There are numerous approaches for

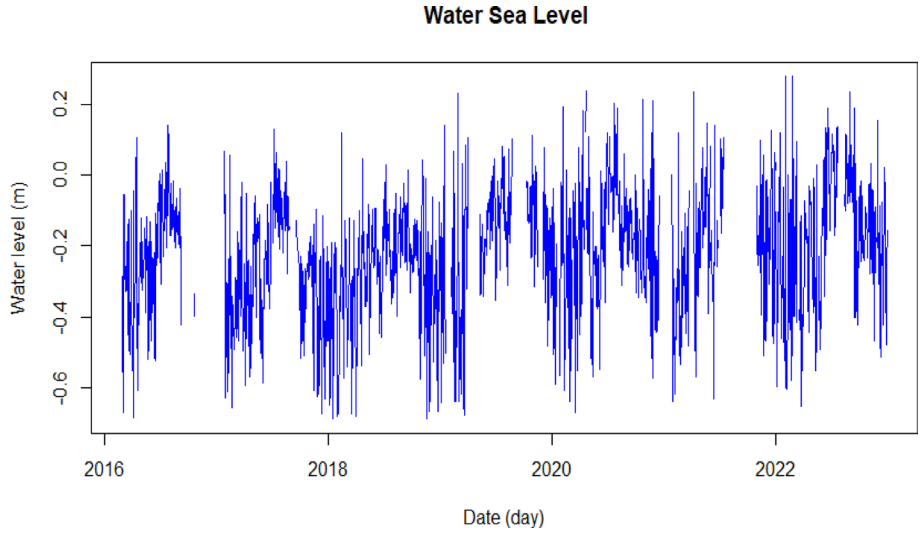

Fig. 3 Daily time series of the water level in Northwest tip of Arabian Gulf (2016–2022)

measuring model performance, and this study used three commonly accepted indicators. Mean Squared Error (MSE) calculates the differences between predicted and actual values, penalizing larger errors more heavily. Root Mean Square Error (RMSE) is the square root of MSE, representing the standard deviation of prediction error; however, it is scale-dependent, making it suitable for coming time series with different unite. Mean Absolute Error (MAE) measures the average of absolute differences between predicted and actual values, expressed in the same units as the data, making it scale- independent and suitable for model comparison across datasets with consistent units [56]. These measures, determined using Eqs. (1-2-3, where $\boldsymbol{Y_t}$ represents the actual value and $\bar{\boldsymbol{Y}}_{\boldsymbol{t}}$ the anticipated value for time t [56], provide insights into forecasting model performance. In addition, n denotes the total number of observations.

$$\boldsymbol{MSE} = \frac{1}{\boldsymbol{n}} \sum_{\boldsymbol{t}=1}^{\boldsymbol{n}} \left(\boldsymbol{Y_t} - \bar{\boldsymbol{Y}}_{\boldsymbol{t}} \right)^2 \tag{1}$$

$$RMSE = \sqrt{MSE} \tag{2}$$

$$MAE = \frac{1}{n} \sum_{t=1}^{n} \left| \frac{\left(Y_t - \bar{Y}_t \right)}{Y_t} \right| \tag{3}$$

4.3 Data partitioning

Evaluating model performance in machine learning mostly depends on splitting data into training and testing sets. This technique guarantees generalizability to extrapolations and helps to prevent overfitting with training data. But time series data requires a time-based split because of natural temporal relationships [62]. Common in many fields, random splitting would throw off these relationships and cause erroneous assessments.

Using a common approach, this work allocates 20% of the data to the testing set and 80% to the training set. This split reserves enough data for a strong assessment [41, 50] and balances training the model on a significant volume.

5 Forecasting models

5.1 ARIMA and SARIMA models

The Autoregressive Integrated Moving Average (ARIMA) model, introduced by Box and Jenkins (1970), is a widely used method for time-series forecasting. It combines autoregressive and moving average components, making it particularly suitable for non-stationary time-series data by integrating them to achieve stationarity.

In the ARIMA model, the future value y_t is determined as a linear combination of past values and random errors, represented as:

$$\begin{aligned} y_t \; &= \; \theta_0 \; + \; \phi_1 \; y_{t-1} \; + \phi_2 \; y_{t-2} \\ &+ \; \ldots \; + \; \phi_p \; y_{t-p} \; + \; \varepsilon_t - \; \theta_1 \varepsilon_{t-1} \; - \; \theta_2 \varepsilon_{t-2} \\ &- \; \ldots \; - \; \theta_q \varepsilon_{t-q} \end{aligned} \tag{4}$$

In this context, y_t represents the value that will occur in the future, whereas p and q represent the autoregressive (AR) and moving average (MA) polynomials, respectively. The character ϵ_t represents the error, while θ_i and φ_i denote the coefficients.

The ARIMA model can be extended to handle seasonal time-series data using the Seasonal ARIMA (SARIMA) model, denoted as ARIMA(p, d,q)(P, D,Q)$_m$. Here, p, d, and q represent orders of non- seasonal components, and P, D, and Q denote orders of seasonal components, with m defining the length of the seasonal cycle.

The SARIMA model, is tailored explicitly for univariate time series data, extending the capabilities of ARIMA to accommodate time series data with seasonal patterns. It introduces three additional parameters to account for the seasonal autoregressive (AR), differencing (I), and moving average (MA) components, along with an extra parameter to specify the seasonality period.

The SARIMA(p, d, q)(P, D, Q)s model is formulated as follows [57] :

$$\varphi_p(B)\ \Phi_P\left(B^S\right)(1-B)^d((1-B^S)^D y_t\ =\ \theta_q(B)\,\Theta_Q\left(B^S\right)\epsilon_t \tag{5}$$

$$\left(1-\sum_{i=1}^{p}\phi_i B^i\right)\left(1-\sum_{k=1}^{P}\Phi_k B^{kS}\right)y_t$$
$$=\ \left(1-\sum_{j=1}^{q}\theta_j B^j\right)\left(1-\sum_{l=1}^{Q}\theta_l B^{lS}\right)\ \varepsilon_t$$

Where:

y_t represents the observation value at time t.
ϵ_t represents the random error at time t, with $\epsilon_t \sim NID\ (0,\ \sigma_\epsilon^2)$.
$\varphi_p(B)$ is the non-seasonal autoregressive operator of order p.
$\theta_q(B)$ is the non-seasonal moving average operator of order q.
$\Phi_P\left(B^S\right)$ is the seasonal autoregressive operator of order P with period S.
$\Theta_Q\left(B^S\right)$ is the seasonal moving average operator of order Q with period S.

5.2 Long short-term memory networks (LSTM)

The Long Short-Term Memory (LSTM), a type of recurrent neural network, is widely used in time-series forecasting [58]. It features three primary gates: the forget gate, input gate, and output gate. Mathematically, the LSTM structure is described by the following equations:

$$f_t = \sigma_g(W_f x_t + U_f h_{t-1} + b_f)$$
$$i_t = \sigma_g(W_i x_t + U_{fi} h_{t-1} + b_i) \tag{6}$$
$$o_i = \sigma_g(W_0 x_t + U_0 h_{t-1} + b_0)$$

$$c_t = f_t \odot c_{t-1} + i_t \odot \sigma_c(W_c x_t + U_c h_{t-1} + b_c)$$
$$h_t = o_t \odot \sigma_h(C_t)$$

The activation vectors of the forget gate, input gate, and output gate are represented by the symbols ,f_t , i_t and in this particular case. Furthermore, h_t and c_t represent the hidden state vector and the cell state vector, respectively. The weight matrices and bias vector are denoted by W, U, and b, respectively.

When predicting time-series data using LSTM, it is frequently recommended to standardize the dataset to guarantee that its values are scaled between 0 and 1. The importance of this standardization arises from the significant sensitivity of LSTM models to the data's magnitude. After the preparation of the dataset, the LSTM model is developed and trained. The transformation of the time-series data into unsupervised format is critical step in developing an LSTM model using the Keras library. This process reformulates the data such that the observation at time step *t-1* serves as the input, while the observation at time step *t* is used as the output. To streamline this conversion, the Timeseries Generator library is employed, enabling the efficient preparation of time-series data for supervised learning applications [59]. The LSTM model architecture employs a succession of specialized layers to capture temporal dependencies in time series data. It starts with an input layer that processes sequences of historical data. The core LSTM layer, which has 50 units, maintains a memory cell state using gating methods, allowing the model to retain and use information over long time. A dropout layer with a 0.5 rate is included to mitigate overfitting by randomly omitting neurons during training. The prediction is output from the final dense layer. The Adam optimizer is used to improve the model, which has an exponentially decaying learning rate. The loss function is Mean Squared Error (MSE).

5.3 Convolutional neural network (CNN)

This study also leverages Convelotional Neural Networks (CNN), a class of deep neural networks primarily utilized for tasks such as image analysis and nutural language processing. CNNs are characterized by their use of one or more convolutional layers, which are designed to extract meaningful patterns and features from data [60]. However, its capacity to spot trends makes it useful in forecasting as well. The following CNN layer consumes the outputs from earlier CNN layers. The max-pooling layer stops the model from overfitting [61]. and absorbs the most number in the sliding window. One uses a flattening layer between this layer and the thick layer. With 1D convolutional layer [62], Fig. 4 presents a standard CNN design. The CNN architecture begins with an input layer

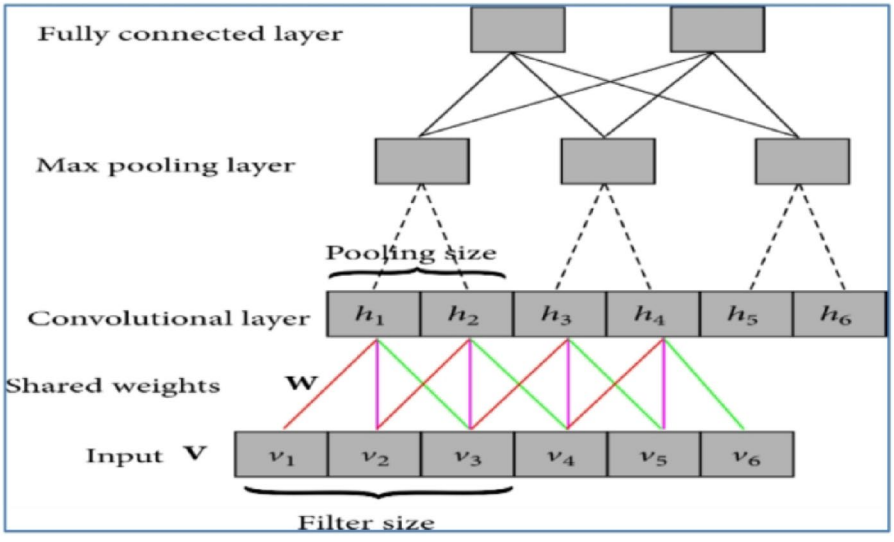

Fig. 4 Typical CNN architecture using 1D convolutions [64]

that handles 10-step sequences, and the multivariate model includes other meteorological variables. Following a MaxPooling layer with a pool size of two, both models have a 1D convolutional layer with 64 filters and a kernel size of 3. After pooling, the models use a Flatten layer to transform the 3D feature maps to 1D vectors. A thick layer of 50 neurons and ReLU activation follow this. The final output layer contains a single neuron with a linear activation function, which is suitable for predicting Sea level variations.

5.4 Combined CNN-LSTM model

The combined CNN-LSTM model is a hybrid model that combines the best features of both CNN and LSTM [63]. This creates a model that is adaptable and flexible, able to capture complicated patterns and variations in time series data. The merging of CNN and LSTM for time series forecasting provides significant advantages. The incorporation of CNN layers in the model allows for the automatic extraction of relevant patterns and features from the input time series data. CNNs' resilience to noise and volatility makes them perfect for use with real-world data. Furthermore, LSTM networks capture long-term dependencies and temporal relationships, enhancing the model's ability to retain crucial information over extended sequences. Overall, integrating the CNN and LSTM offers more accurate and reliable predictions by effectively uniting local and global information and capturing both short-term fluctuations and long-term trends. The CNN component of the combined CNN-LSTM model has the following parts: an input layer for processing sequences of historical data, a 1D convolutional layer including 64 filters with a kernel size of 3, a max-pooling layer with a pool size of two, and subsequent flattening into a 1D vector. Following this, dense layers are modified to fit the sequence duration. The LSTM architecture includes an input layer with alike sequence data, a 50-unit LSTM layer, and dense layers culminating in a single output neuron. Before the final prediction, the outputs from the CNN and LSTM parts are concatenated and further processed through extra dense layers.

6 Results and discussion

The outcomes are discussed in this section. The first five and a half years of water level history make up the training set that each model is trained on. The remaining data, equivalent to the last 1.5 years of water level history, is utilized for testing each model.

6.1 Traditional statistical methods (ARIMA and SARIMA)

There are many methods accessible to select the most optimal hyperparameters for a model. In both ARIMA and SARIMA models, Grid Search might be used in addition to generating Autocorrelation Function (ACF) and Partial Autocorrelation Function (PACF) plots The ACF plot for the original data is presented in Fig. 3, which shows the autocorrelation structure of the series. We also applied the Augmented Dickey-Fuller test to examine trend/stationarity. As the series was non-stationary ($p < 0.05$), first differencing (d = 1) was applied to achieve stationarity before fitting ARIMA/SARIMA models. For the first differenced data, the ACF plot in Fig. 4 reveal key patterns: a gradual decay toward zero after a few lags and the presence of a seasonal structure. These observations suggest that the data may be well-suited for an ARIMA(p, d, q) model, where the values of p and q are yet to be determined. To identify the optimal configuration of

Table 1 Parameters of ARIMA (1,1,1) model

Parameter	Estimate	SE	Z	$P > \|Z\|$
Differencing	1			
AR Lag 1 ($\varnothing_1$)	0.463	0.022	21.38	0.00
MA Lag 1 (θ_1)	-0.936	0.011	-86.46	0.00

Table 2 Parameters of SARIMA(3,1,1) (1,1,0,12) model

Parameter	Estimate	SE	Z	$P > \|Z\|$
Differencing	1			
AR Lag 1 ($\varnothing_1$)	0.591	0.020	28.86	0.00
AR Lag 1 ($\varnothing_2$)	-0.211	0.023	-9.12	0.00
AR Lag 1 ($\varnothing_3$)	0.119	0.022	5.31	0.00
MA Lag 1 (θ_1)	-1.00	0.188	-5.32	0.00
SAR Lag 1 ($\varnothing_1$)	-0.475	0.019	-25.31	0.00

hyperparameters, we used Grid Search—a systematic approach that evaluates different combinations of hyperparameters. The performance of each model was assessed based on the Akaike Information Criteria (AIC) and Bayesian Information Criteria (BIC), as shown in Figs. 6 and 7. Both criteria provide a measure of the model's fit, with the goal of minimizing these values to select the best model Table 1, 2.

The formulas for AIC and BIC are as follows:

$$\mathrm{AIC} = -2\log(\text{maximum likelihood}) + 2\mathrm{k} \tag{7}$$

$$\mathrm{BIC} = -2\log(\text{maximum likelihood}) + \mathrm{k}\log(\mathrm{n}) \tag{8}$$

Where k is the number of parameters in the model (p + q or p + q + 1 if an intercept term is used).

According to the normalized AIC and BIC values, the most appropriate ARIMA model is ARIMA (1,1,1).

$$\widehat{Y}_t = -0.463Y_{t-1} - 0.936\mathrm{e}_{t-1}$$

Since the data has seasonal pattern as shown in Fig. 5, it is important to consider the seasonal part in the appropriate ARIMA model. In the given scenario, after examining several models, the SARIMA (3,1,1) (1,1,0,12) model was identified as the best fit based on the lowest BIC value.

The parameters of the model, including the order of the autoregressive (AR), differencing (I), and moving average (MA) components for both the non-seasonal and seasonal parts, are presented in Table 3. These parameters were determined through the iterative process of fitting various SARIMA models and evaluating their BIC values .

The SARIMA (3,1,1)(1,1,0,12) model for the data can be expressed as follows:

$$\widehat{Y}_t = 0.591Y_{t-1} - 0.211Y_{t-2} + 0.1191Y_{t-3} - 1.0\mathrm{e}_{t-1} - 0.475Y_{t-12}$$

In the context of ARIMA and SARIMA models, it is essential to examine various assumptions regarding the residuals. These assumptions include stationarity, independence, normality, and homoscedasticity. For both the ARIMA(1,1,1) and SARIMA(3,1,1) (1,1,0,12) models, diagnostic tests were conducted to evaluate these assumptions and ensure the models' validity. Figure 7 presents the diagnostic tests and plots for the

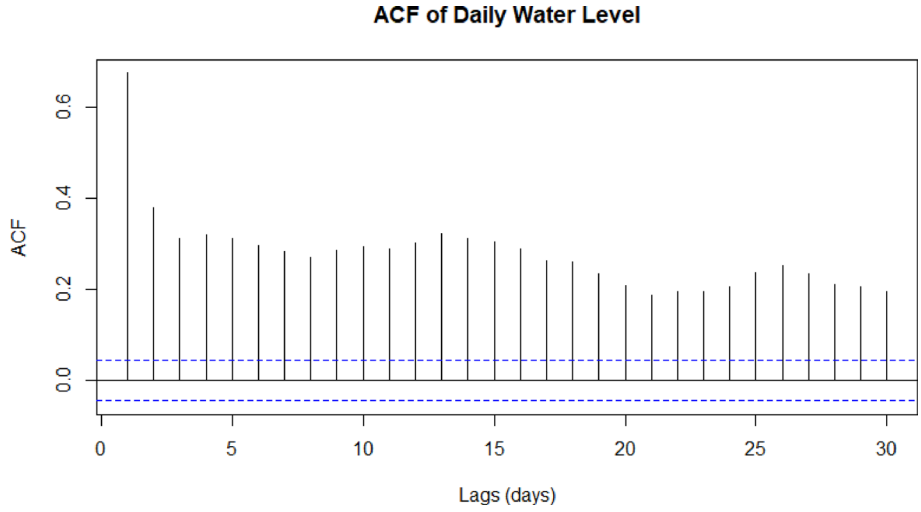

Fig. 5 ACF for the original time series data of daily water level

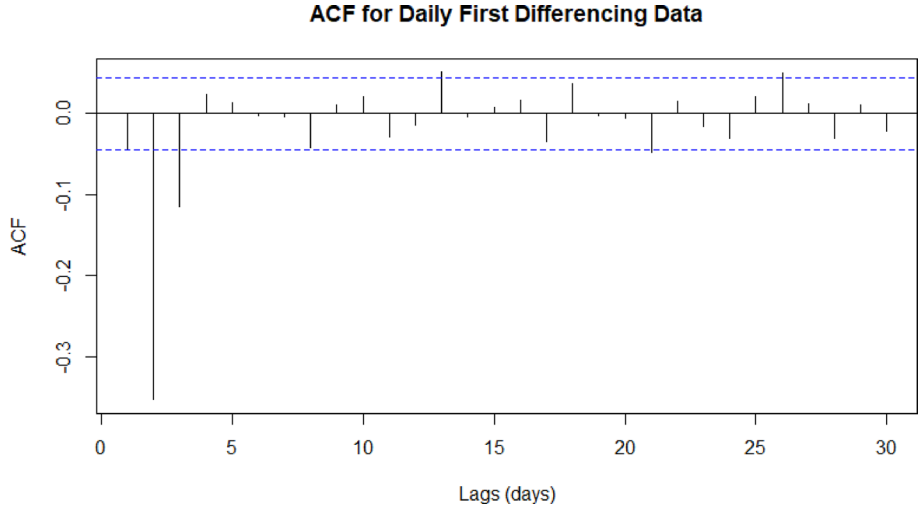

Fig. 6 ACF for the first differencing for the data of water level (2016–2022)

Table 3 Performance metrics for statistic and DL models

Model	MSE	RMSE	MAE
SARIMA	0.0265	0.1626	0.1288
CNN	0.0191	0.1384	0.1126
LSTM	0.0172	0.1311	0.1055
CNN-LSTM	0.0165	0.1282	0.1015

residuals of the ARIMA(1,1,1) model, while Fig. 8 illustrates the corresponding tests for the SARIMA(3,1,1)(1,1,0,12) model. The results of the diagnostic analysis revealed that all key assumptions were satisfied for both models. The analysis revealed that all the residual assumptions were satisfied for both models. The residuals demonstrated stationarity, as evidenced by the ACF plot and Ljung-Box Q-test [64] (Ljung and Box, 1978). There was no indication of seasonality or autocorrelation in the residuals. Moreover, the histogram plot of the residuals displayed a roughly normal distribution, meeting the

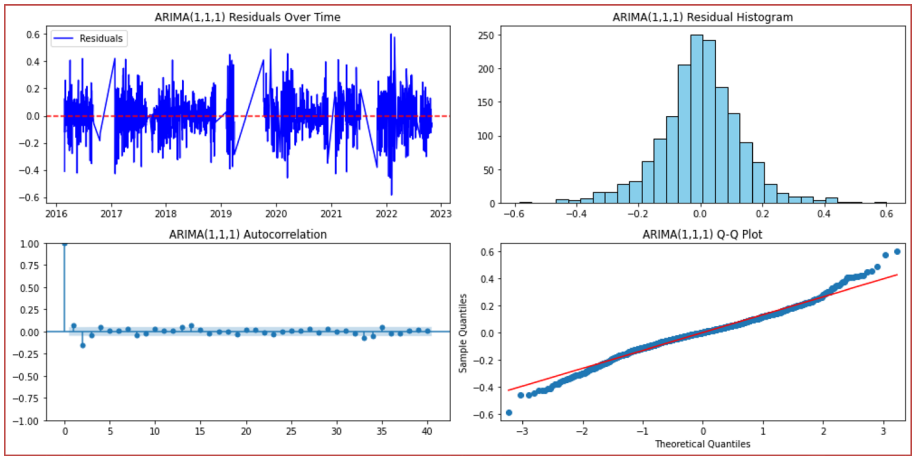

Fig. 7 Diagnostic plots of ARIMA (1,1,1) model

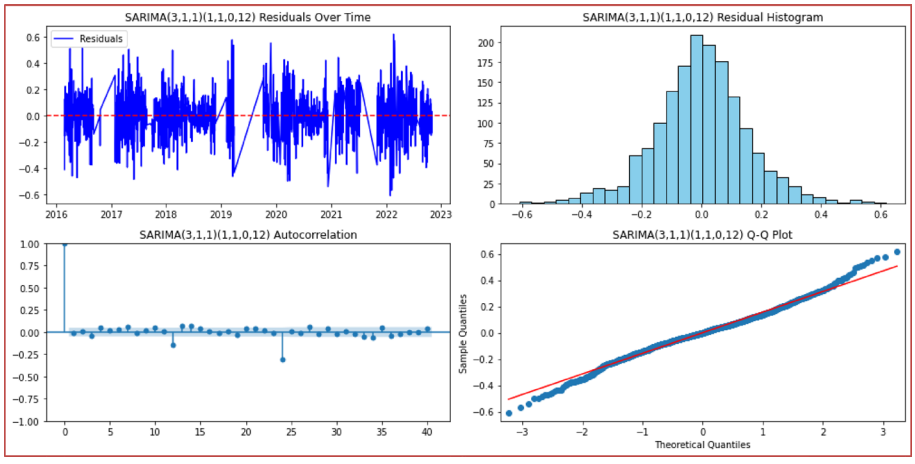

Fig. 8 Diagnostic plots of SARIMA (3,1,1) (1,1,0,12) model

assumption of normality. Additionally, the variance of the residuals appeared to be constant over time, indicating homoscedasticity.

These findings provide assurance and increase our confidence in the outcomes and forecasts generated by the ARIMA (1,1,1) and SARIMA (3,1,1) (1,1,0,12) allowing for reliable predictions and forecasts.

Based on the analysis conducted, the ARIMA (1,1,1) and SARIMA (3,1,1) (1,1,0,12) models have been identified as the most suitable models for predicting sea levels in the.

Northwest Arabian Gulf over a 7-year period from 2016 to 2022. However, among the ARIMA variants discussed, ARIMA (1,1,1) does not emerge as a superior choice, as it fails to match the future predictions of water levels accurately.

In contrast, the SARIMA(3,1,1)(1,1,0,12) model exhibited superior long-term forecasting capability. It performed significantly better than the ARIMA model, as evidenced by its ability to capture future water level trends more accurately. This performance is clearly demonstrated in Fig. 7, which shows the SARIMA model's robust predictions compared to the ARIMA model's less reliable forecast Fig. 9.

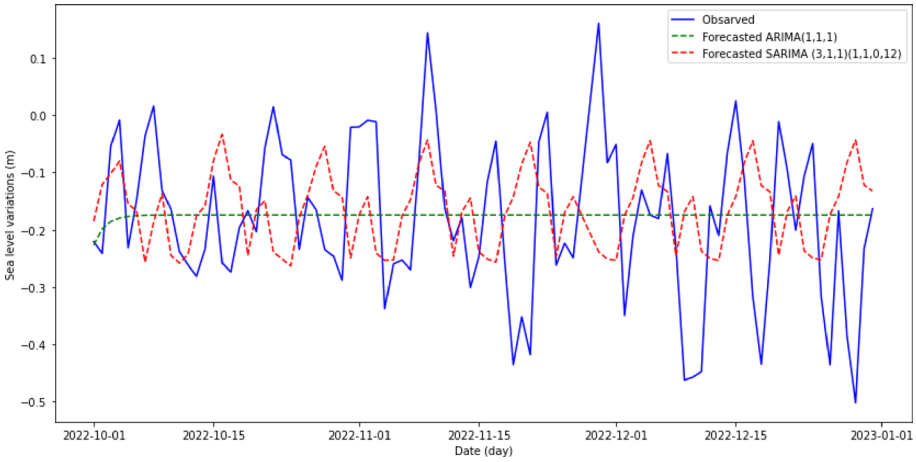

Fig. 9 Comparison the predicting values of SARIMA model with the observed SLV

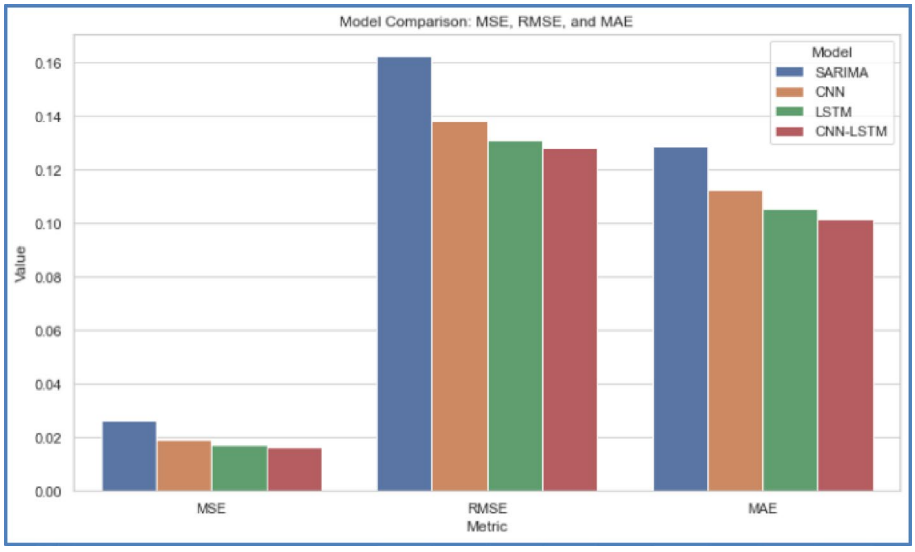

Fig. 10 Bar plot comparing the performance metrics (MSE, RMSE, and MAE) of each model

6.2 Machine learning and deep learning models

In this study, three distinct artificial intelligence approaches Convolutional Neural Networks (CNNs), Long Short-Term Memory (LSTM) models, and a combined CNN-LSTM model were employed to predict future sea level variations (SLV) using historical SLV data. The results of these models demonstrate their superior predictive capabilities compared to traditional statistical approaches such as SARIMA. In this study, three distinct artificial intelligence approaches Convolutional Neural Networks (CNNs), Long Short-Term Memory (LSTM) models, and a combined CNN-LSTM model were employed to predict future sea level variations (SLV) using historical SLV data. The results of these models demonstrate their superior predictive capabilities compared to traditional statistical approaches such as SARIMA. This is summarized in Table 3 and further illustrated by the bar plot of performance metrics (MSE, RMSE, and MAE) in Fig. 10, which highlights the insights gained from each model.

6.2.1 Convolutional neural networks (CNNs)

The CNN model demonstrated better predictive performance than the SARIMA model, as evidenced by improved evaluation metrics presented in Table 3 CNN's ability to capture spatial hierarchies within the data likely contributed to its enhanced performance over SARIMA, which relies on linear dependencies.

A graphical comparison of the CNN-predicted SLV values and observed SLV data is provided in Fig. 11, which illustrates that the CNN model effectively captures the primary patterns of SLV fluctuations.

6.2.2 Long short-term memory LSTM model

The LSTM model outperformed both the CNN and SARIMA models, as shown in Table 3. This superior performance is expected given LSTM's capability to process sequential data and recognize complex temporal dependencies.

LSTMs excel at maintaining long-term dependencies and capturing non-linear relationships, making them particularly suitable for time series data like SLV. The results, depicted in Fig. 12, show that the LSTM model produces predictions that align closely with observed SLV values, effectively capturing both short- and long-term patterns in sea level fluctuations.

6.2.3 Combined CNN & LSTM models

Among all the models tested, the combined CNN-LSTM model demonstrated the most accurate predictive performance, achieving the highest evaluation metrics as shown in Table 3. This model leverages the strengths of both CNNs—capable of capturing spatial hierarchies—and LSTMs, which excel at modeling temporal dependencies. The hybrid nature of this model allows it to effectively capture the intricate patterns and fluctuations of SLV over time.

Figure 13 illustrates the CNN-LSTM model's predictions compared to observed SLV data. Additionally, Fig. 14 provides a comprehensive comparison of predictions across all models, including SARIMA, CNN, LSTM, and CNN-LSTM. This visual comparison highlights the robust performance of the CNN-LSTM model, which aligns most closely with the observed SLV data and captures sea level fluctuation patterns effectively.

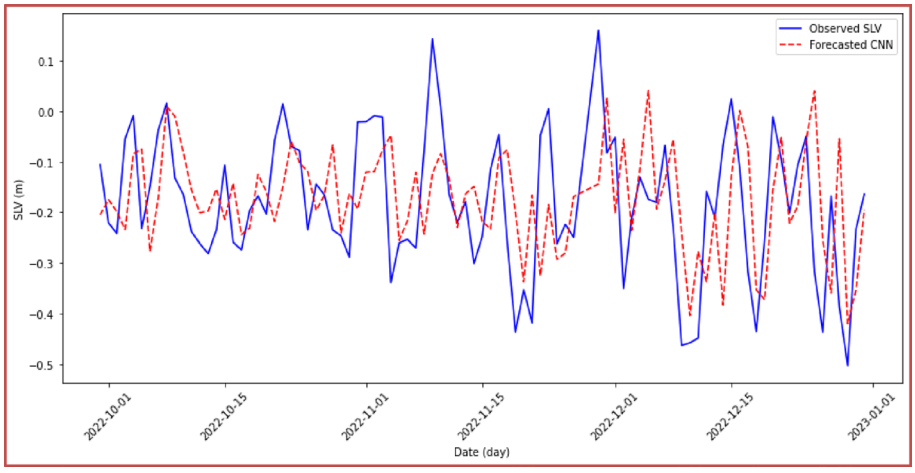

Fig. 11 Comparison the predicting values of CNN model with the observed SLV

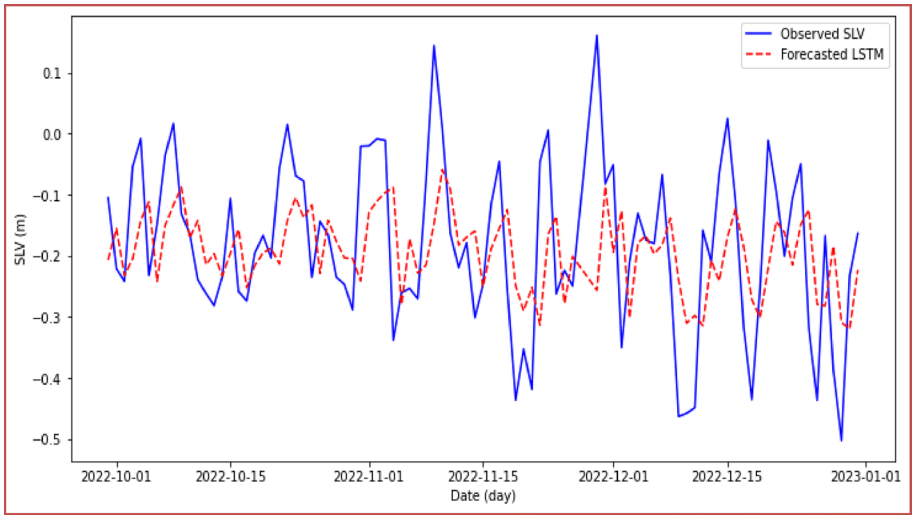

Fig. 12 Comparison the predicting values of LSTM model with the observed SLV

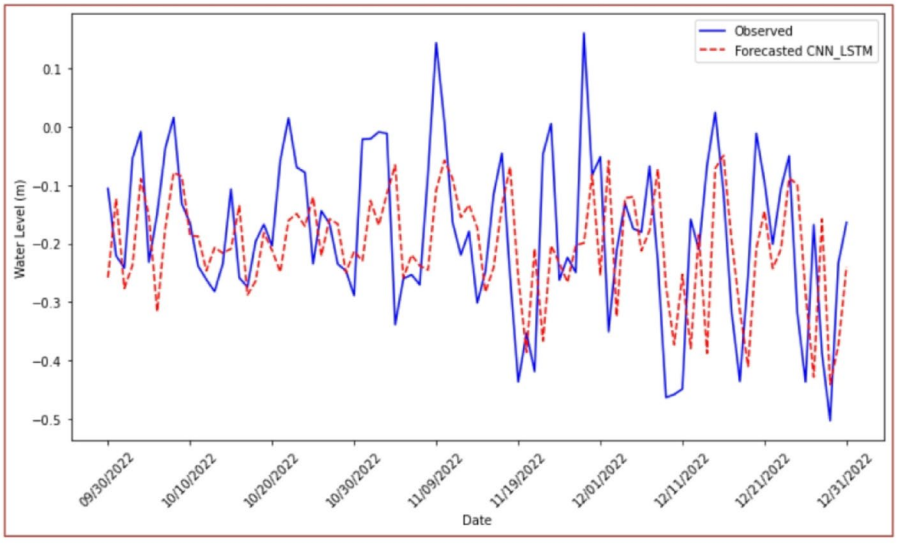

Fig. 13 Comparison the predicting values of combined CNN_LSTM model with the observed SLV

The CNN and LSTM models also demonstrate strong predictive capabilities, matching observed SLV patterns to a significant extent. However, the CNN-LSTM model consistently provides the most precise representation over time. On the other hand, the SARIMA model, while producing acceptable forecasts, shows noticeable deviations from the observed SLV.

The results illustrated in Fig. 14 emphasize the superiority of advanced deep learning methods, particularly the hybrid CNN-LSTM model, in predicting complex and nonlinear sea level variations. This finding underscores the potential of these models for improving forecasting accuracy, contributing to better-informed decision-making in coastal management and climate adaptation planning.

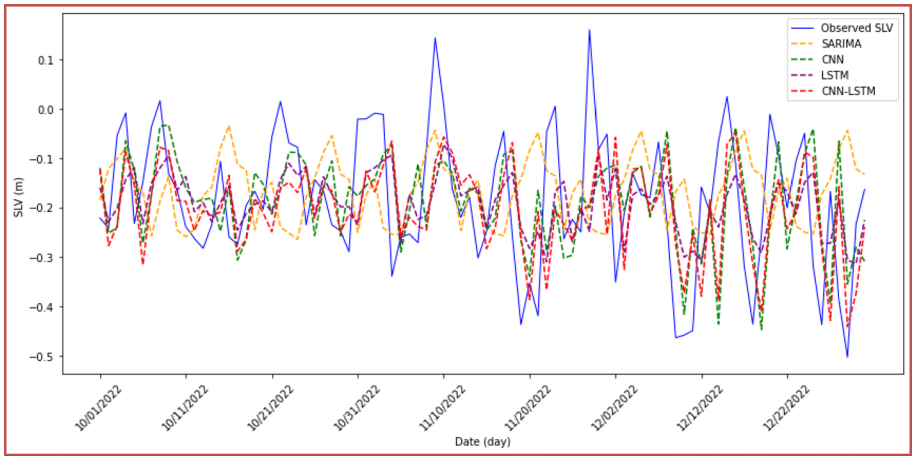

Fig. 14 Comparison of model predictions against observed SLV data

7 Conclusion

Forecasting sea level variations is inherently challenging due to the complex interplay of variables that influence tides, including global warming, storm surges, and the motions and positions of celestial bodies, particularly the Earth-Moon-Sun relationship. This study investigated statistical and deep learning approaches to forecast sea level variations in the northwestern Arabian Gulf. A comprehensive evaluation compared statistical models (ARIMA and SARIMA) with advanced deep learning models, including CNNs, LSTM networks, and a hybrid CNN-LSTM architecture. The results revealed that deep learning models significantly outperformed the SARIMA model in predictive accuracy, as evidenced by performance metrics such as MSE, RMSE, and MAE. Among these methods, the CNN-LSTM model emerged as the most accurate and resilient for forecasting sea level variations. The findings of this research have important implications for flood hazard estimation and disaster risk management in coastal regions. However, it is important to acknowledge that the forecast results are not entirely free from uncertainties. External factors and variables not accounted for in the models—such as meteorological variables, ocean currents, precipitation, geological processes, and salinity—represent limitations to the current approach. Future studies should explore the integration of these additional variables to further enhance predictive accuracy. In conclusion, this study bridges traditional statistical forecasting methods with modern deep learning techniques, providing a more precise and reliable framework for sea level predictions. The findings enhance our understanding of sea level changes in the northwestern Arabian Gulf and offer a foundation for improving forecasting methodologies in similar coastal regions.

7.1 Limitations and future work

This study is limited to univariate forecasting utilizing historical sea-level data without the inclusion of meteorological or oceanographic variables. While the deep learning models (LSTM, CNN, and CNN-LSTM) demonstrated powerful predictive performance, their accuracy could likely be improved by incorporating relevant environmental predictors. Future research should explore multivariate modeling approaches that integrate meteorological factors and test hybrid frameworks that combine statistical

and machine learning techniques. Such improvements may further enhance forecasting accuracy and strengthen early warning systems for coastal flood risk management.

Another limitation is that the study focused on retrospective modeling using data up to 2022 and did not extend to long-term future forecasting. Future research should incorporate the most recent observational data and explore the application of these models for seasonal to interannual forecasts, which could provide valuable insights for coastal planning and risk management.

Acknowledgements
The author expresses gratitude to the Basra University/ Marine Science Center/ Marine Physic Department and General Company of Iraq Ports and General Acoustics, Germany, particularly to Eng. Jörg Stuczynski for providing the data.

Author contributions
A.J.B.A. conceptualized the study, data acquisition, preprocessing, and validation, performed data analysis, developed the SARIMA and deep learning models, and wrote the main manuscript text. J.V. supervised the research, and contributed to manuscript revisions. P.R. assisted with statistical modeling, data interpretation and contributed to manuscript revisions. A.L. contributed to data collection and preprocessing. All authors reviewed and approved the final manuscript.

Funding
This research was supported in part by the University of Basra, Iraq. No additional funding, grants, or financial support were received for conducting this study or preparing this manuscript.

Data availability
The tidal and oceanographic data used in this study were collected from an offshore measurement platform located approximately 655 m from the western breakwater of Faw Grand Port, established by the General Company of Iraq Ports and DAEWOO Engineering and Construction. The data is managed by General Acoustics (Germany) ([https://www.generalacoustics.com](https:/www.generalacoustics.com)). This dataset, covering the period 2016–2022 with 10-minute interval recordings, is not publicly available but can be accessed upon request through the General Company of Iraq Ports. Additional processed data supporting the findings of this study are available from the corresponding author upon reasonable request.

Declarations

Ethics approval and consent to participate
Not applicable. This study is based solely on environmental/oceanographic data and does not involve human participants, animals, or sensitive materials.

Consent for publication
Not applicable. This study does not include personal data, images, or identifiable information.

Competing interests
The authors declare no competing interests.

Received: 16 March 2025 / Accepted: 30 September 2025
Published online: 08 October 2025

References

1. Bevacqua E, Vousdoukas MI, Zappa G, Hodges K, Shepherd TG, Maraun D, Mentaschi L, Feyen L. More meteorological events that drive compound coastal flooding are projected under climate change. Commun Earth Environ. 2020;1(1):47.
2. Hirabayashi Y, Mahendran R, Koirala S, Konoshima L, Yamazaki D, Watanabe S, Kim H, Kanae S. Global flood risk under climate change. Nat Clim Change. 2013;3(9):816–21.
3. Jongman B, Ward PJ, Aerts JC. Global exposure to river and coastal flooding: long term trends and changes. Glob Environ Change. 2012;22(4):823–35.
4. Vitousek S, Barnard PL, Fletcher CH, Frazer N, Erikson L, Storlazzi CD. Doubling of coastal flooding frequency within decades due to Sea-Level rise. Sci Rep. 2017;7(1):1399.
5. Irani M, Naderi MM, Bavani M, Hassanzadeh AR, E., and, Moftakhari H. A framework for coastal flood hazard assessment under sea level rise: application to the Persian Gulf. J Environ Manage. 2024;349:119502. https://doi.org/10.1016/j.jenvman.2023.119502.
6. Reynolds RM. Physical oceanography of the Gulf, Strait of Hormuz, and the Gulf of Oman—Results from the Mt Mitchell expedition. Mar Pollut Bull. 1993;27:35–59. https://doi.org/10.1016/0025-326X(93)90007-7.
7. Alosairi Y, Imberger J, Falconer RA. 2011, Mixing and Flushing in the Arabian/Persian Gulf. J Geophys Res C Oceans, 116.
8. Kämpf J, Sadrinasab M. The circulation of the Persian gulf: A numerical study. Ocean Sci. 2006;2(1):27–41.
9. Ranjbar MH, Etemad-Shahidi A, Kamranzad B. Modeling the combined impact of climate change and sea-Level rise on general circulation and residence time in a Semi-Enclosed sea. Sci Total Environ. 2020;740:140073.
10. Pattiaratchi CB, Wijeratne E. Are meteotsunamis an underrated hazard? Philos Trans R Soc Math Phys Eng Sci. 2015;373(2053):20140377.
11. Heidarzadeh M, Šepić J, Rabinovich A, Allahyar M, Soltanpour A, Tavakoli F. Meteorological tsunami of 19 March 2017 in the Persian gulf: observations and analyses. Pure Appl Geophys. 2020;177:1231–59.

12. Din E. S. S., 1990, Sea level variation along the Western Coast of the Arabian Gulf. Int Hydrogr Rev.
13. Sultan S, Ahmad F, Elghribi N, Al-Subhi A. An analysis of Arabian Gulf monthly mean sea level. Cont Shelf Res. 1995;15(11–12):1471–82.
14. Hosseinibalam F, Hassanzadeh S, Kiasatpour A. Interannual variability and seasonal contribution of thermal expansion to sea level in the Persian Gulf. Deep Sea Res Part Oceanogr Res Pap. 2007;54(9):1474–85.
15. Al-Subhi AM. 2010, Tide and sea level characteristics at Juaymah, West Coast of the Arabian Gulf. Mar Scienes, 21(1).
16. Lafta AA, Altaei SA, Al-Hashimi NH. 2019, Characteristics of the tidal wave in Khor Abdullah and Khor Al-Zubair Channels, Northwest of the Arabian Gulf. Mesopotamian J Mar Sci, 34(2).
17. Alenezi N, Alsulaili A, Alkhalidi M. 2023, Prediction of Sea Level in the Arabian Gulf Using Artificial Neural Networks, J. Mar. Sci. Eng., 11(11), p. 2052.
18. Elneel L, Zitouni MS, Mukhtar H, Al-Ahmad H. Examining sea levels forecasting using autoregressive and prophet models. Sci Rep. 2024;14(1):14337.
19. Goh C, Law R. Modeling and forecasting tourism demand for arrivals with stochastic nonstationary seasonality and intervention. Tour Manag. 2002;23(5):499–510. https://doi.org/10.1016/S0261-5177(02)00009-2.
20. Williams BM, Hoel LA. Modeling and forecasting vehicular traffic flow as a seasonal ARIMA process: theoretical basis and empirical results. J Transp Eng. 2003;129(6):664–72.
21. Box GE, Jenkins GM, Reinsel GC, Ljung GM. Time series analysis: forecasting and control. Wiley; 2015.
22. Hipel KW, McLeod AI. 1994, *Time Series Modelling of Water Resources and Environmental Systems*, Elsevier Science; Developments in Water Science, 45. [Online]. Available: https://search.ebscohost.com/login.aspx?direct=true%26db=edselc%26AN=edselc.2-52.0-85003034722%26site=eds-live%26scope=site%26custid=s1181350%26group=main%26profid=eds%26authtype=ip,guest
23. Cryer JD, Chan K-S. 2008, Seasonal models. Time Ser Anal Appl R, pp. 227–48.
24. Selvaraj JJ, Arunachalam V, Coronado-Franco KV, Romero-Orjuela LV, Ramírez-Yara YN. Time-Series modeling of fishery landings in the Colombian Pacific ocean using an ARIMA model. Reg Stud Mar Sci. 2020;39:101477. https://doi.org/10.1016/j.rsma.2020.101477.
25. Anbarasan M, Muthu B, Sivaparthipan CB, Sundarasekar R, Kadry S, Krishnamoorthy S, Dasel AA. Detection of flood disaster system based on IoT, big data and convolutional deep neural network. Comput Commun. 2020;150:150–7.
26. Pan J, Yin Y, Xiong J, Luo W, Gui G, Sari H. Deep Learning-Based unmanned surveillance systems for observing water levels. Ieee Access. 2018;6:73561–71.
27. Ahmadlou M, Al-Fugara A, Al-Shabeeb AR, Arora A, Al-Adamat R, Pham QB, Al-Ansari N, Linh NTT, Sajedi H. Flood susceptibility mapping and assessment using a novel deep learning model combining multilayer perceptron and autoencoder neural networks. J Flood Risk Manag. 2021;14(1):e12683.
28. Amershi S, Begel A, Bird C, DeLine R, Gall H, Kamar E, Nagappan N, Nushi B, Zimmermann T. 2019, Software Engineering for Machine Learning: A Case Study, *2019 IEEE/ACM 41st International Conference on Software Engineering: Software Engineering in Practice (ICSE-SEIP)*, IEEE, pp. 291–300.
29. Konakoglu B, Aydemir SB, Kutlu Onay F. Application of a metaheuristic Gradient-based optimizer algorithm integrated into artificial neural network model in a local geoid modeling with global navigation satellite Systems/Leveling measurements. Concurr Comput Pract Exp. 2022;34(18):e7017.
30. Dimiduk DM, Holm EA, Niezgoda SR. Perspectives on the impact of machine Learning, deep Learning, and artificial intelligence on Materials, Processes, and structures engineering. Integrating Mater Manuf Innov. 2018;7:157–72.
31. Elshambaky HT, Kaloop MR, Hu JW. A novel Three-Direction datum transformation of geodetic coordinates for Egypt using artificial neural network approach. Arab J Geosci. 2018;11:1–14.
32. Alpaydin E. Introduction to machine learning. MIT Press; 2020.
33. Gensler A, Henze J, Sick B, Raabe N. Deep learning for solar power Forecasting—An approach using autoencoder and LSTM neural networks. 2016 IEEE Int Conf Syst Man Cybernetics (SMC). 2016;IEEE:002858–65.
34. Zhuge Q, Xu L, Zhang G. 2017, LSTM neural network with emotional analysis for prediction of stock price. Eng Lett, 25(2).
35. Zhao Z, Chen W, Wu X, Chen PC, Liu J. LSTM network: A deep learning approach for Short-term traffic forecast. IET Intell Transp Syst. 2017;11(2):68–75.
36. Gu J, Wang Z, Kuen J, Ma L, Shahroudy A, Shuai B, Liu T, Wang X, Wang G, Cai J, Chen T. Recent advances in convolutional neural networks. Pattern Recognit. 2018;77:354–77. https://doi.org/10.1016/j.patcog.2017.10.013.
37. Sorkhabi OM, Milani M. Deep learning of ionosphere Single-Layer model and tomography. Geomagn Aeron. 2022;62(4):474–81.
38. Li Z, Liu F, Yang W, Peng S, Zhou J. A survey of convolutional neural networks: Analysis, Applications, and prospects. IEEE Trans Neural Netw Learn Syst. 2021;33(12):6999–7019.
39. Koprinska I, Wu D, Wang Z. 2018, Convolutional Neural Networks for Energy Time Series Forecasting, *2018 International Joint Conference on Neural Networks (IJCNN)*, IEEE, pp. 1–8.
40. Momeny M, Latif AM, Sarram MA, Sheikhpour R, Zhang YD. A noise robust convolutional neural network for image classification. Results Eng. 2021;10:100225.
41. Sorkhabi OM, Shadmanfar B, Al-Amidi MM. Deep learning of Sea-Level variability and flood for coastal City resilience. City Environ Interact. 2023;17:100098.
42. Amalou I, Mouhni N, Abdali A. Multivariate time series prediction by RNN architectures for energy consumption forecasting. Energy Rep. 2022;8:1084–91.
43. Fischer T, Krauss C. Deep learning with long Short-Term memory networks for financial market predictions. Eur J Oper Res. 2018;270(2):654–69.
44. Graves A, Graves A. 2012, Long Short-Term memory. Supervised Seq Label Recurr Neural Netw, pp. 37–45.
45. Muhammad AU, Djigal H, Muazu T, Adam JM, Ba AF, Dabai US, Tijjani S, Yahaya MS, Ashiru A, Kumshe UMM, Aliyu S, Richard FA. An Autoencoder-Based stacked LSTM transfer learning model for EC forecasting. Earth Sci Inf. 2023;16(4):3369–85. https://doi.org/10.1007/s12145-023-01096-3.
46. Balogun A-L, Adebisi N. Sea level prediction using ARIMA, SVR and LSTM neural network: assessing the impact of ensemble Ocean-Atmospheric processes on models' accuracy. Geomat Nat Hazards Risk. 2021;12(1):653–74.
47. Uluocak I. Comparative study of multivariate hybrid neural networks for global sea level prediction through 2050. Environ Earth Sci. 2025;84(3):79. https://doi.org/10.1007/s12665-025-12090-x.

48. Uluocak I, Pinar E, Bilgili M. Atmospheric NO2 concentration prediction with statistical and hybrid deep learning methods. Environ Ecol Stat. 2025;32(1):89–118. https://doi.org/10.1007/s10651-024-00637-3.
49. Lafta AA, Al-Fartusi AJ. General characteristics of surface waves in Iraq marine Water, Northwest of Arabian Gulf. Arab J Geosci. 2022;15(20):1598.
50. Lafta AA, Altaei SA, Al-Hashimi NH. Impacts of potential Sea-Level rise on tidal dynamics in Khor Abdullah and Khor Al-Zubair, Northwest of Arabian Gulf. Earth Syst Environ. 2020;4(1):93–105. https://doi.org/10.1007/s41748-020-00147-9.
51. Teubner MD, Najafi HS, Noye BJ, Rasser PE. 1999, Modelling Tides in the Persian Gulf Using Dynamic Nesting, *Modelling Coastal Sea Processes*, World Scientific, pp. 57–80.
52. Zakaria E, Solfitri T, Daud Y, Abidin ZZ. Effect of cooperative learning on secondary school students' mathematics achievement. Creat Educ. 2013;4(2):98–100.
53. Lafta AA, Al-Fartusi AJ. General characteristics of surface waves in Iraq marine Water, Northwest of Arabian Gulf. Arab J Geosci. 2022;15(20). https://doi.org/10.1007/s12517-022-10884-y.
54. Lafta AA. General characteristics of tidal currents in the entrance of Khor Abdullah, Northwest of Arabian Gulf. Oceanologia. 2023;65(3):494–502. https://doi.org/10.1016/j.oceano.2023.03.002.
55. Kotzur L, Markewitz P, Robinius M, Stolten D. Impact of different time series aggregation methods on optimal energy system design. Renew Energy. 2018;117:474–87.
56. Hamzaçebi C. Improving artificial neural networks' performance in seasonal time series forecasting. Inf Sci. 2008;178(23):4550–9.
57. Nontapa C, Kesamoon C, Kaewhawong N, Intrapaiboon P. 2020, A New Time Series Forecasting Using Decomposition Method with SARIMAX Model, *Neural Information Processing: 27th International Conference, ICONIP 2020, Bangkok, Thailand, November 18–22, 2020, Proceedings, Part V 27*, Springer, pp. 743–751.
58. Muhammad AU, Abba SI. Earth Sci Inf. 2023;16(2):1241–64. https://doi.org/10.1007/s12145-023-00952-6. Transfer Learning for Streamflow Forecasting Using Unguaged MOPEX Basins Data Set.
59. Ensafi Y, Amin SH, Zhang G, Shah B. Time-series forecasting of seasonal items sales using machine learning – a comparative analysis. Int J Inf Manag Data Insights. 2022;2(1):100058. https://doi.org/10.1016/j.jjimei.2022.100058.
60. Nasir JA, Khan OS, Varlamis I. Fake news detection: a hybrid CNN-RNN based deep learning approach. Int J Inf Manag Data Insights. 2021;1(1):100007.
61. Ackermann N. Introduction to 1D convolutional neural networks in Keras for time sequences. Good Audience Front Page Deep Tech; 2018.
62. Hu W, Huang Y, Wei L, Zhang F, Li H. Deep convolutional neural networks for hyperspectral image classification. J Sens. 2015;2015:1–12.
63. Kumshe UMM, Abdulhamid ZM, Mala BA, Muazu T, Muhammad AU, Sangary O, Ba AF, Tijjani S, Adam JM, Ali MAH, Bello AU, Bala MM. Improving short-term daily streamflow forecasting using an autoencoder based CNN-LSTM model. Water Resour Manag. 2024;38(15):5973–89. https://doi.org/10.1007/s11269-024-03937-2.
64. Ljung GM, Box GE. 1980, Analysis of variance with autocorrelated observations. Scand J Stat, pp. 172–80.

Publisher's note